



Considerable asymmetry of the critical current in a niobium thin strip of plano-convex section

G. Carapella, P. Sabatino, and G. Costabile

Citation: *J. Appl. Phys.* **111**, 053912 (2012); doi: 10.1063/1.3692809

View online: <http://dx.doi.org/10.1063/1.3692809>

View Table of Contents: <http://jap.aip.org/resource/1/JAPIAU/v111/i5>

Published by the [American Institute of Physics](#).

Related Articles

Experimental realization of superconducting quantum interference devices with topological insulator junctions
Appl. Phys. Lett. **100**, 072602 (2012)

Long range supercurrents in ferromagnetic CrO₂ using a multilayer contact structure
Appl. Phys. Lett. **100**, 052602 (2012)

Determination of critical current density from arbitrary flux relaxation process
AIP Advances **2**, 012125 (2012)

Flux pinning properties of correlated pinning at low temperatures in ErBCO films with inclined columnar defects
J. Appl. Phys. **111**, 013914 (2012)

Measurements and calculations of transport AC loss in second generation high temperature superconducting pancake coils
J. Appl. Phys. **110**, 113906 (2011)

Additional information on *J. Appl. Phys.*


Journal Homepage: <http://jap.aip.org/>

Journal Information: http://jap.aip.org/about/about_the_journal

Top downloads: http://jap.aip.org/features/most_downloaded

Information for Authors: <http://jap.aip.org/authors>

ADVERTISEMENT

	Working @ low temperatures? Contact Janis for Cryogenic Research Equipment Click here to browse our site at www.janis.com	
---	---	---

Considerable asymmetry of the critical current in a niobium thin strip of plano-convex section

G. Carapella,^{a)} P. Sabatino, and G. Costabile
 CNR-SPIN and Dipartimento di Fisica “E. R. Caianiello,” Università degli Studi di Salerno,
 I-84084 Fisciano (Sa), Italy

(Received 10 January 2012; accepted 16 February 2012; published online 6 March 2012)

We experimentally demonstrate that in the presence of an in-plane magnetic field the voltage-current curve of a Nb thin strip having plano-convex cross section exhibits considerable asymmetry of the critical current. The observed behavior can be accounted for by the magnetic field component normal to the top convex surface of the strip. Such a component is inhomogeneous, changes sign in the middle of the strip and affects the three-dimensional vortices that in this system have sections locally perpendicular to the top convex surface, though the magnetic field is applied parallel to the bottom flat surface. These sections play the most significant role in the generation of the observed asymmetry. A maximum asymmetry ratio of about 300% at 4.2 K is observed when the strip is in the mixed state and can be ascribed to the balance of the magnetic force due to the inhomogeneous field component and the polarity dependent Lorentz force associated to the transport current. © 2012 American Institute of Physics. [<http://dx.doi.org/10.1063/1.3692809>]

I. INTRODUCTION

Asymmetric voltage-current [$V(I)$] curves exhibited by superconducting devices are at the base of superconducting rectifiers, or superconducting diodes,^{1–12}. A superconducting diode is the dual of a semiconducting diode, as the role of current and voltage are interchanged. It exhibits zero or finite resistance depending on the sign of the bias current. Compared to a semiconducting diode, this kind of diode is a rather low impedance device that can support and rectify very high current densities even near the absolute zero. Recently, asymmetric $V(I)$ curves have been reported^{6–12} in ferromagnet-superconductor hybrids on the micron scale. The asymmetry in the critical¹³ currents in these hybrids has often been attributed^{6–12} to the inhomogeneous stray magnetic fields generated by the ferromagnet.

Here we demonstrate experimentally that a marked asymmetry in the critical currents can be also exhibited by a single thin superconducting strip having plano-convex cross section when subjected to a homogeneous magnetic field applied parallel to the substrate. Unlike the ferromagnet-superconductor hybrids, this kind of rectifier does not undergo hysteresis or the bistability phenomena normally associated to a ferromagnetic film, that, though desirable for some applications (e.g., memory elements), could be unwanted in some other applications. Our strip is made of a type II superconductor,¹³ niobium, in the dirty limit regime. Here we report measurements on $V(I)$ curves and asymmetry ratios as function of the applied magnetic field and temperature, besides an example of rectification of an AC current.

From the physical point of view, here we are concerned with the magneto-transport properties of a superconducting thin strip with curved and asymmetric cross section, a subject relatively unexplored until now. We will show, with the help of

numerical simulations performed in the framework of the full three-dimensional (3D) time dependent Ginzburg Landau (TDGL) model, that the asymmetry can be mainly accounted for by the magnetic field component normal to the convex top surface. Such a component is inhomogeneous, being antisymmetric with respect to the middle of the strip, and affects the flux entry and flux exit. Here the flux consists of 3D vortices that have sections locally perpendicular to the top convex surface, though the bulk section, when present, is parallel to the applied magnetic field and to the bottom flat surface. These sections play the most significant role in the generation of the observed asymmetry. We anticipate that the result of the analysis can be summarized as follows. At low magnetic fields (Meissner state) the asymmetry comes from the balance of the normal component of the magnetic field and the polarity dependent self-field of the transport current. At larger magnetic fields (mixed state) the asymmetry comes from the balance of the magnetic force due to the inhomogeneous normal component of field and the polarity dependent Lorentz force associated to the transport current.

The work is organized as follows. In Sec. II, after a brief description on how the Nb strip with plano-convex section is fabricated, we report the main experimental results on asymmetry of critical currents as well as an example of rectification of an AC current. In Sec. III the observed asymmetry in magneto-transport properties of the superconducting strip is explained with the help of numerical simulations performed in the framework of time-dependent Ginzburg Landau equations,¹³ that are reliably used^{14–19} whenever direct computation of voltage-current curves of a type II superconductor in the presence of magnetic field is needed. A brief summary of main results is given in Sec. IV.

II. EXPERIMENTAL RESULTS

We fabricated a Nb thin strip with convex upper surface by means of rf-sputter deposition through a bilayer resist

^{a)}Electronic mail: giocar@sa.infn.it.

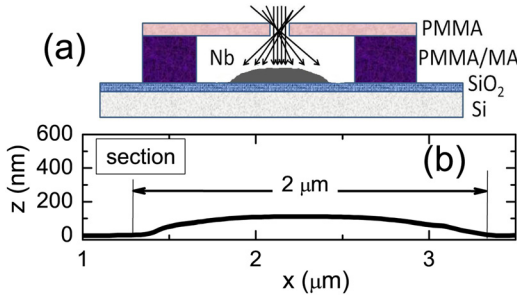


FIG. 1. (Color online) (a) A sketch (not on scale) of the bilayer resist mask used to sputter Nb. (b) AFM profile of the Nb strip along its width.

shadow mask²⁰ [see Fig. 1(a)] made by electron beam lithography (EBL). The resist bilayer consisted of a 0.2 μm thick layer of polymethylmethacrylate (PMMA) and a 0.7 μm thick layer of PMMA-copolymer (PMMA/MA). A 1 μm wide strip is patterned on the bilayer with an area dose of 100 $\mu\text{C}/\text{cm}^2$. Due to the remarkable difference in sensitivity between the two resist layers, a large undercut in the PMMA/MA layer below the PMMA layer is obtained after development, so that the bilayer can work as a shadow mask [see Fig. 1(a)]. To enhance resistance to plasma, after development the mask is further baked at 130 $^\circ\text{C}$ for 30 min in a convection oven. Moreover, to minimize resist contamination,²⁰ prior to the deposition of the strip a 10 nm thick Nb passivation layer is first sputtered and allowed to relax to passivate the resist surface. Due to the isotropy of the sputter process, the Nb is smeared under the window formed by the top layer of resist, resulting in a smoothly graded profile for the Nb deposited on the Si/SiO₂ substrate, as sketched in Fig. 1(a). The profile of the Nb strip recorded with an atomic force microscope (AFM) confirms the expected plano-convex (bottom surface is flat and top surface is convex) shape, as shown in Fig. 1(b). The sample has a four contact geometry, with voltage pads 10 μm apart. The Nb strip is 2 μm wide and is 100 nm thick in the middle [see Fig. 1(b)].

In Fig. 2(a) we show the $V(I)$ curve of the strip recorded at $T = 4.2\text{ K}$ ($T_c = 6.0\text{ K}$) with a magnetic field $\mu_0 H = 0.2\text{ T}$ applied parallel to the substrate and perpendicular to the transport current, as sketched in the inset. In the reference frame shown in the inset, the magnetic field is directed as the x -axis, $\mathbf{H} = (H, 0, 0)$, and the current density as the y -axis, $\mathbf{J} = (0, J, 0)$. The positive and the negative depairing currents¹³ [I_{DP} and I_{DN} , the current values at which the transition to the fully normal state takes place, see arrows in Fig. 2(a)] are found to be moderately different and the positive and negative critical currents¹³ [I_{CP} and I_{CN} , the current values corresponding to the transition $V = 0 \rightarrow V \neq 0$, see arrows in the bottom panel of Fig. 2(a)] are found to be remarkably different, as emphasized in the bottom panel of Fig. 2(a). The $V(I)$ curves are mirrored with respect to the origin when the magnetic field polarity is reversed [Fig. 2(b)], therefore, in the following we will show data concerning only the positive magnetic fields. The critical currents, estimated using a 0.2 μV criterion, and the depairing currents as a function of magnetic field are shown in Fig. 2(c). The maximum asymmetry ratio [Fig. 2(d)] for the depairing currents is $100 \times (I_{DP} - |I_{DN}|)/|I_{DN}| = 40\%$ and is $100 \times (I_{CP} - |I_{CN}|)/|I_{CN}| = 300\%$ for the critical currents.

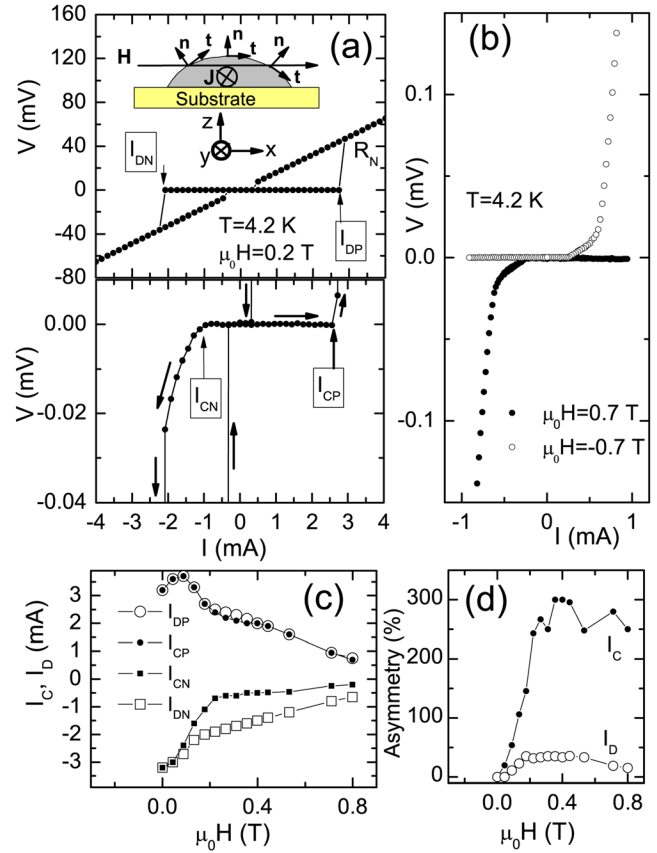


FIG. 2. (Color online) (a) $V(I)$ curve of the strip with the identification of the depairing currents. The magnetic field is applied as sketched in the inset. In the bottom panel the magnification of the low voltage region emphasizes the difference between the critical currents. The arrows indicate the history of the voltage-current loop. (b) $V(I)$ curves at magnetic fields of opposite polarities. Positive and negative depairing and critical currents [(c)], and asymmetry ratio [(d)] as a function of magnetic field.

From Fig. 2(c) we notice that, at the chosen polarity of magnetic field, the positive critical current I_{CP} is always larger than the negative critical current I_{CN} . Moreover, though at large magnetic field values the positive critical current is depressed as the magnetic field is increased, at low magnetic fields an opposite behavior is observed, i.e., the critical current is enhanced with respect to the zero magnetic field value. The enhancement, that at 4.2 K is of about 30% reaches 60% at lower temperatures as can be appreciated in Fig. 3(a), where we compare the $V(I)$ curve at zero field with the one at $\mu_0 H = 0.18\text{ T}$, both recorded at 0.3 K. The critical currents and their asymmetry ratio as a function of magnetic field at this temperature are plotted in Fig. 3(b). The asymmetry ratios in Figs. 2(d) and 3(b) indicate that maximum asymmetry is always achieved at relatively high magnetic field values, where both critical currents are depressed with respect to the zero field value. Nevertheless, the qualitative difference in the positive critical current trend at low fields with respect to the large fields values suggests that there can be two different mechanisms at the origin of the asymmetry, depending on the field range. In Fig. 3(c) we show some $V(I)$ curves recorded near the critical temperature $T_c = 6.0\text{ K}$ at a fixed value of the applied magnetic field. A considerable asymmetry is observed in a large temperature range,

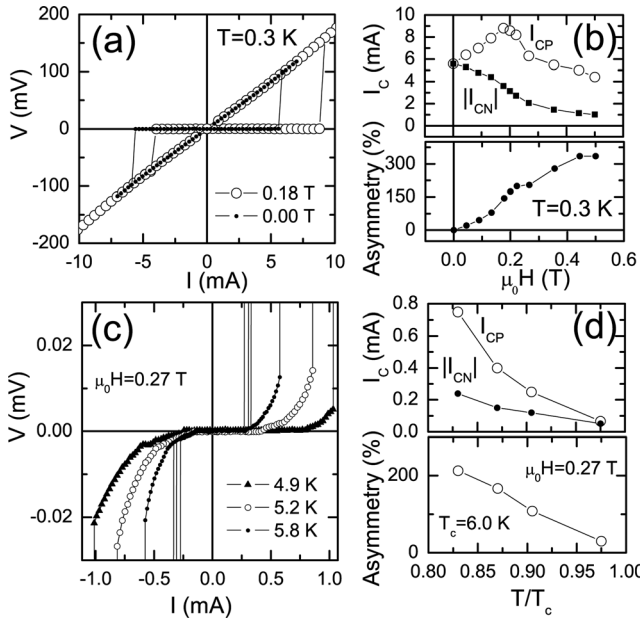


FIG. 3. (a) $V(I)$ curve of the strip in zero magnetic field compared with the curve at $\mu_0 H = 0.18$ T, emphasizing enhancement of positive critical current (almost coincident with the positive depairing current). The temperature is 0.3 K. (b) Positive and negative critical currents (top panel), and asymmetry ratio (bottom panel) as a function of magnetic field, at $T = 0.3$ K. (c) $V(I)$ curves recorded near the critical temperature T_c at a fixed magnetic field. (d) Positive and negative critical currents (top panel), and asymmetry ratio (bottom panel) as a function of temperature, at fixed field $\mu_0 H = 0.27$ T.

reaching vanishingly small values only at $T/T_c \approx 0.98$, as can be better appreciated in Fig. 3(d), where we plotted the critical currents as function of reduced temperature T/T_c at a fixed field.

Finally, the asymmetry is practically absent if the magnetic field is applied perpendicular to the substrate, as shown in the Fig. 4(a), where we report some $V(I)$ curves recorded at different magnetic fields at 4.2 K. For this field orientation, besides some vanishingly small asymmetry of the voltages probably accounted for by the not perfect symmetry of the strip profile around its middle point [see Fig. 1(b)], the critical currents are found to be reasonably symmetric within 10% accuracy, as can be appreciated in Fig. 4(b).

Due to the asymmetry of depairing or critical currents, our strip in parallel magnetic field can exhibit a zero or finite resistance depending on the direction of the bias current.

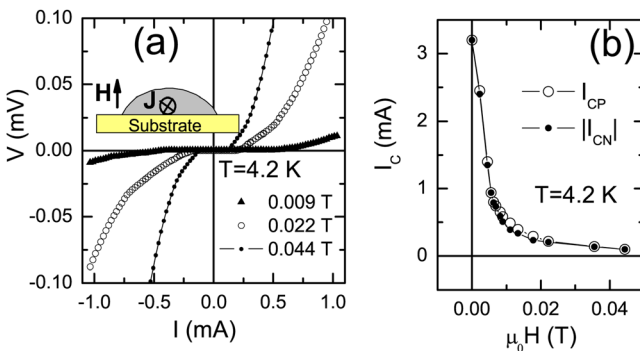


FIG. 4. (Color online) (a) $V(I)$ curves at $T = 4.2$ K at different magnetic fields applied perpendicular to the substrate, as shown in the inset. (b) Critical currents as a function of magnetic field applied as in (a), at 4.2 K.

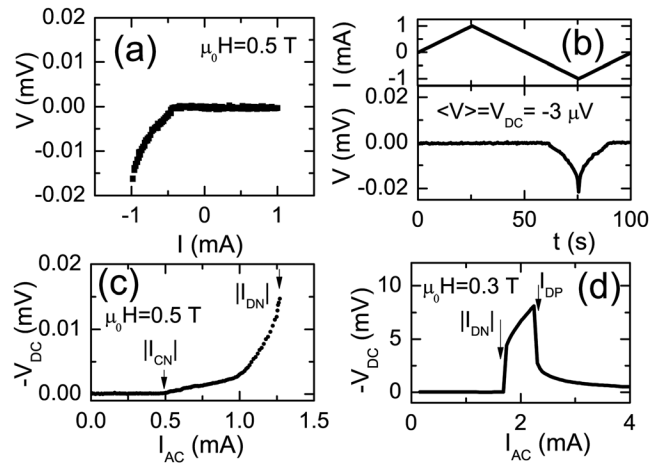


FIG. 5. (a) $V(I)$ curve of the strip at 4.2 K subjected to an in-plane magnetic field of $\mu_0 H = 0.5$ T. (b) Time traces of forcing current and output voltage corresponding to $V(I)$ curve in (a). (c) DC voltage output as a function of the amplitude of a sinusoidal driving current of 1 kHz. (d) Same as in (c), but the range of the AC current amplitude is larger and the field is $\mu_0 H = 0.3$ T.

This behavior is evidenced in Fig. 5(a), where we plot the $V(I)$ curve of the strip recorded at $\mu_0 H = 0.5$ T: at $I = 1$ mA the resistance is zero, while at $I = -1$ mA the resistance is finite (though quite low, few percent of $R_N \approx 17 \Omega$). The curve in Fig. 5(a) was recorded at $T = 4.2$ K driving the strip with a low frequency triangular current $I(t)$ with amplitude $-I_{CN} < I_{AC} < I_{CP}$ [see top panel of Fig. 5(b)], measuring the voltage $V(t)$ [see bottom panel of Fig. 5(b)], then eliminating the time. The time average of the current is $\langle I(t) \rangle = 0$ but the time average of the output voltage is $\langle V(t) \rangle \neq 0$, i.e., our strip behaves as a current rectifier. It is worth noticing that the current density here is rather large, of the order of 10 GA/m^2 , as should be expected for a superconducting device. A way to characterize the rectification capability^{3,5} of the strip is to plot the time average of the output voltage $\langle V(t) \rangle \equiv V_{DC}$ as a function of the amplitude I_{AC} of AC driving current. An example of such a $V_{DC}(I_{AC})$ curve at $\mu_0 H = 0.5$ T is shown Fig. 5(c). This curve is recorded driving the device with a sinusoidal signal at 1 kHz with amplitude I_{AC} while stepping to progressively larger values of I_{AC} and measuring the voltage at each amplitude with a DC nano-voltmeter. In this case, the V_{DC} is in the μV range and it is achieved for $|I_{CN}| < I_{AC} < I_{CP}$, due to the difference in the critical currents. In Fig. 5(d) the field is $\mu_0 H = 0.3$ T and the AC current amplitude is in a wider range. Here rectification when V_{DC} increased up to the mV range occurs for $|I_{DN}| < I_{AC} < I_{DP}$, because now the finite resistance involved is the normal state resistance R_N . Notice that, though the normal state is approached with high current density, dissipative heating is minimized, because the sample is immersed in liquid helium and is in the resistive state only during a small fraction of the signal cycle.

III. NUMERICAL RESULTS AND DISCUSSION

From the profile shown in Fig. 1(b) we notice that the top surface of the strip can be approximated by a cylindrical surface having a curvature radius $R \approx 4 \mu\text{m}$. In the experiment the magnetic field is applied parallel to the cord of the

arc, as shown in the inset of Fig. 2(a). Though the applied magnetic field \mathbf{H} is homogeneous, both the component H_n normal and the component H_t tangent to the top surface are inhomogeneous, but the H_n is qualitatively different, because it changes sign in the middle of the strip and can probably explain the asymmetry. In fact, the analysis we present below substantially confirms this hypothesis.

From the slope close to T_c of the upper critical field $\mu_0 H_{c2}(T)$ we estimate²¹ for our sputtered Nb thin film a coherence length $\xi(0) \simeq 9$ nm. This value is much smaller than the BCS coherence length of Nb, $\xi_0 = 39$ nm, so the sample is in the dirty limit regime with an electron mean free path $l = 1.38\xi(0)^2/\xi_0 \simeq 2.8$ nm. In the dirty limit regime the Ginzburg-Landau parameter can be estimated by $\kappa = 0.72\lambda_L/l \simeq 10$, with $\lambda_L = 40$ nm the London penetration depth of Nb. This result implies that the investigated sample is a type-II superconductor. The Ginzburg-Landau London penetration depth is $\lambda(0) = \kappa\xi(0) = 90$ nm, that is of the order of the thickness d of our strip at its middle. Normalized relevant physical dimensions of the strip are $W \simeq 222\xi(0)$, $d \simeq 11\xi(0)$, $L = 5W$ and $R \simeq 2W$.

To gain insight in the origin of asymmetric magneto-transport properties of our superconducting strip with plano-convex section, we performed numerical simulations in the framework of the time-dependent Ginzburg-Landau (TDGL) model^{14–19} in the full three-dimensional version (3D model). The full 3D model with realistic parameters is computationally very expensive. Hence, we have used this model only as a guide to individuate the main mechanism for the asymmetry.

The celebrated three-dimensional time-dependent Ginzburg-Landau (TDGL) model^{14–19} reads:

$$u \frac{\partial \psi}{\partial t} = (\nabla - i\mathbf{A})^2 \psi + (1 - T - |\psi|^2) \psi, \quad (1)$$

$$\frac{\partial \mathbf{A}}{\partial t} = \frac{1}{2i} (\psi^* \nabla \psi - \psi \nabla \psi^*) - |\psi|^2 \mathbf{A} - \kappa^2 \nabla \times (\nabla \times \mathbf{A} - \mathbf{H}). \quad (2)$$

Here $\psi = \psi(x, y, z)$ is the complex order parameter, $\mathbf{A} = (A_x, A_y, A_z)$ is the vector potential, \mathbf{H} is the applied magnetic field, T is the temperature, κ is the Ginzburg-Landau parameter and the coefficient $u = 5.79$ controls the relaxation of ψ . All physical quantities are measured in dimensionless units: the coordinates are in units of the coherence length $\xi(0) = \sqrt{\pi \hbar D / 8 k_B T_c}$, with T_c the critical temperature, and D is the diffusion constant. Temperature is in units of T_c . Time is measured in units of the relaxation time $\tau(0) = 4\pi\sigma_n \lambda(0)^2 / c^2$ (σ_n is the normal-state conductivity, $\lambda(0) = \kappa\xi(0)$ the magnetic field penetration depth, with κ the G-L parameter). The order parameter is in units of $\Delta(0) = 4k_B T_c \sqrt{u} / \pi$, i.e., the superconducting gap at $T = 0$ which follows from Gor'kov's derivation of the Ginzburg-Landau equations. The vector potential is measured in units $\Phi_0 / 2\pi\xi(0)$ ($\Phi_0 = ch/2e$ is the quantum of magnetic flux). In these units the magnetic field is scaled with $H_{c2}(0) = \Phi_0 / 2\pi\xi(0)^2$ and the current density with $j_0(0) = c\Phi_0 / 8\pi^2 \lambda(0)^2 \xi(0)$. We use the model as stated in Ref. 15, but our normalization is relative to the variables at $T = 0$. This

results in the explicit inclusion of normalized temperature T in the first equation, as found, e.g., in Refs. 18 and 19. The first equation governs the relaxation of the superconducting order parameter ψ and the second equation is the Maxwell equation for magnetic induction field $\mathbf{B} = \nabla \times \mathbf{A}$.

Equations (1) and (2) are integrated in the three-dimensional rectangular domain shown in Fig. 6(a), with external boundary $\partial\bar{\Omega}$. The superconducting material occupies the plano-convex cylindrical region Ω and it is surrounded by vacuum. The boundary $\partial\Omega$ of Ω is the interface between the superconductor and the vacuum. As in the experiment, in the Cartesian reference frame shown in Fig. 6(a) the applied magnetic field is directed as the x -axis, $\mathbf{H} = (H, 0, 0)$, and the transport current density as the y -axis, $\mathbf{J} = (0, J, 0)$. Notice that in this reference frame, is $\nabla \times \mathbf{H} = 0$ and the applied magnetic field only appears in the boundary condition of the vector potential. This condition is chosen such that magnetic induction field $\mathbf{B} = \nabla \times \mathbf{A}$ on the outer boundary goes to the applied field \mathbf{H} when the outer boundary is chosen reasonably far from the superconductor, meaning that screening current does not modify sensibly the applied field at large distances from the superconductor. Mathematically, the condition reads:^{16,22} $(\nabla \times \mathbf{A})|_{\partial\bar{\Omega}} = \mathbf{H}$. When a transport current is present, we add¹⁶ to the applied magnetic field \mathbf{H} also the field \mathbf{H}_f induced by the bias density current \mathbf{J} , calculated using the Biot-Savart law. For the order parameter, we use the superconductor-insulator boundary conditions, i.e., we set the normal component of the supercurrent across the boundary $\partial\Omega$ to zero¹³: $(\nabla - i\mathbf{A})\psi \cdot \mathbf{n}|_{\partial\Omega} = 0$, where \mathbf{n} is the outward normal unit to the surface $\partial\Omega$. Finally, to simulate a infinite length strip, we apply periodic boundary conditions

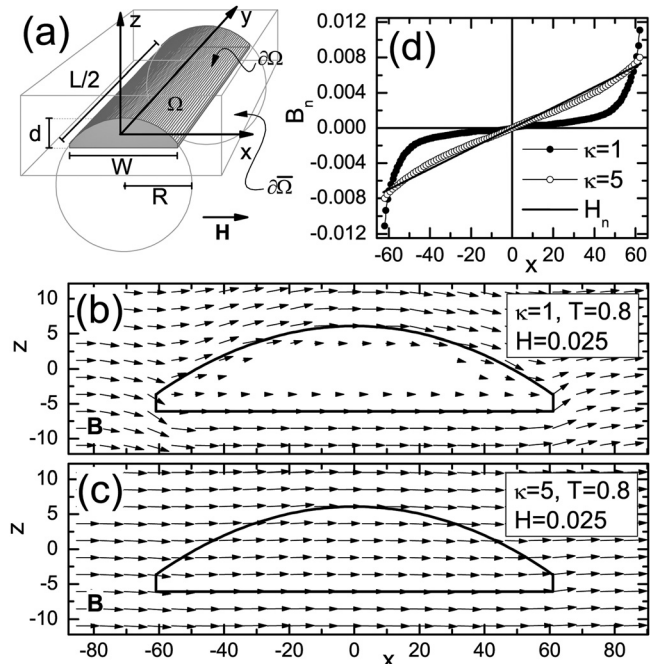


FIG. 6. (a) Sketch the superconducting strip placed in an insulating (vacuum) rectangular box. (b) and (c) show the vector plots of the magnetic induction field for two values of κ , when a weak magnetic field is applied parallel to the bottom surface. (d) Component of the magnetic induction field along the outer normal of the convex surface (B_n) compared the same component of applied magnetic field (H_n).

in the y -direction: $\psi(x, y - \Lambda/2, z) = \psi(x, y + \Lambda/2, z)$ and $\mathbf{A}(x, y - \Lambda/2, z) = \mathbf{A}(x, y + \Lambda/2, z)$, where Λ is the spatial period along y -direction.

To numerically solve the system of Eqs. (1) and (2) we apply a finite-difference representation for the order parameter and vector potential on a uniform Cartesian space grid with step size 0.5 and we use the link variable approach^{15,16} and the simple Euler method²³ with time step $\Delta t = 0.002$ to find ψ and \mathbf{A} . Initial conditions are $|\psi| = 1$ in the region Ω , $|\psi| = 0$ outside, and $\mathbf{A} = 0$ everywhere. The behavior of the system is studied on a large time scale when time-averaged values no longer depend on time. In our calculations we choose parameters $\kappa = 5$, $T = 0.8$, $W = 122$, $R = 1.6W$, thickness at middle $d = 12$, and the spatial period along y -direction $\Lambda = 20$. These parameters, comparable though not the same as in the experiment, were chosen to take into account the efficiency of our computing tools while saving the relevant features. Here we are only interested on main physical mechanism accounting for the observed asymmetry and we are not interested in quantitative fitting of experimental data with numerical data. Moreover, we remark that reduced temperature $T/T_c = 0.8$, chosen to qualitatively account for most significant experimental results summarized in Fig. 2, though relatively far from T_c , is not beyond the range of validity of Ginzburg-Landau theory, because¹⁸ we are concerned with a type II superconductor in the dirty limit, compelling a large κ parameter.

In Figs. 6(b) and 6(c) we show the vector plots of the calculated magnetic induction field \mathbf{B} for two type-II superconductors of same dimensions but with different κ subjected to a magnetic field applied parallel to the bottom surface. In both cases we are in the Meissner state. When κ is small [see Fig. 6(b), $\kappa = 1$] the magnetic field is completely expelled from the bulk of the superconductor (full Meissner screening), and the field lines near the external surface of the strip follow the profile of the strip. Increasing κ , the magnetic field almost completely penetrates the superconductor (very weak screening) and the field lines are almost aligned with the applied magnetic field [see Fig. 6(c), $\kappa = 5$]. This is not surprising if we remember that the strips have different thickness in units of magnetic penetration length λ . At the used temperature $T = 0.8$ the thickness of the strip with $\kappa = 1$ is $d \approx 6\lambda$, allowing a substantial screening of the external magnetic field. Conversely, for the strip with $\kappa = 5$ is $d \approx 1\lambda$ (our experimental strip at this temperature is also more thin, $d \approx 0.5\lambda$), and screening of applied magnetic field is very weak. In Fig. 6(d) the component of magnetic induction normal to the convex top surface, B_n , is compared with the normal component of the applied magnetic field, H_n . Consistently, the screening of this component is rather evident when $\kappa = 1$ and very weak when $\kappa = 5$. Moreover, the modification of the induction field (here an enhancement at the edges of the strip) with respect to the applied field, commonly described with a geometry-dependent demagnetizing factor, is quite noticeable in the strip with low κ but almost absent in the other strip. In the following we always use $\kappa = 5$, more comparable with the experimental one, i.e., $\kappa = 10$.

In Fig. 7(a) there is shown the contour plot of the squared order parameter at $H = 0.11$. For this critical

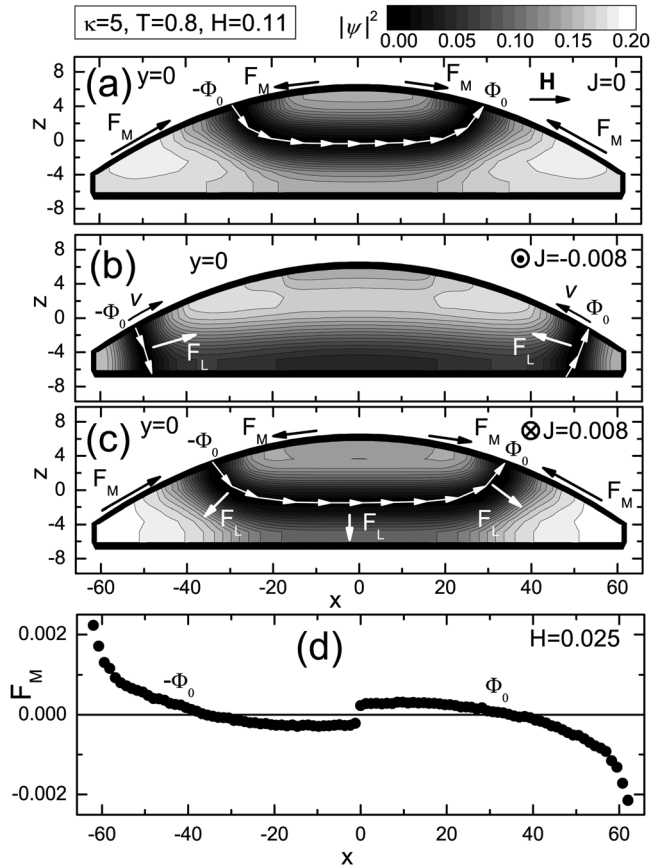


FIG. 7. Contour plots of the squared order parameter at a magnetic field value allowing the first entrance of vortices. Here the section at $y=0$ is shown. In (a) there is no bias current. In (b) is $J = J_{CN}$. In (c) is $J = |J_{CN}| < J_{CP}$. The white arrows indicate direction of the magnetic flux line at the core of the vortex. (d) Local magnetic force acting on the entering piece ($-\Phi_0$, left side of the convex surface of the strip) and exiting piece ($+\Phi_0$, right side of the convex surface of the strip) of the full 3D vortex.

magnetic field value the strip is at onset of the mixed state. Flux enters the strip as 3D vortices that have the bulk section parallel to the applied field, but the lateral sections are perpendicular to the convex top surface, in qualitative agreement with reported numerical results¹⁶ on flux penetration in cylindrical superconductors with field applied perpendicular to the cylinder axis. Moreover, there is also a qualitative agreement with the analytic results on a problem dual with respect to the one we are addressing here, i.e., flux penetration in the case of flat strips with magnetic field tilted with respect to the surface. Also in that case, the vortex was found²⁴ to penetrate perpendicular to the surface despite of tilting, as it happens in our top convex surface, that is locally tilted with respect to the applied field. In Fig. 7(a) only the 3D vortex at section $y=0$ it is shown, for the sake of simplicity. By feeding a transport current density J in the strip, the 3D vortex can be moved by the Lorentz force F_L . In panel (b) we show the effect of a negative transport current density corresponding to the onset of stationary flux motion with associated dissipation, i.e., we are at the negative critical current density $J = J_{CN}$. At this current value, vortex shown in panel (a) is ejected upward because of the F_L and flux enters again as an antivortex (Av) at the left edge and a vortex (V) at the right edge of the strip as shown in panel (b).

This time the bulk section is not present and the 3D V and 3D Av are perpendicular to both top curved surface and bottom flat surface. Under the action of F_L , the V and Av move inward until they join together to form again a vortex as the one in the panel (a). Again, this vortex is expelled from the top surface, continuing the ever dynamic process. In panel (c) we show the effect of application of a positive current density of same modulus as the negative critical current density, $J = |J_{CN}|$. This time the Lorentz force merely shifts down and slightly deforms the 3D vortex of panel (a), but no stationary flux motion is established, meaning no dissipation. To establish dissipation we must feed a positive current larger than the negative critical current. In other words is $J_{CP} > |J_{CN}|$, as in the experiments. However, stationary flux motion is achieved at large enough positive current, $J = J_{CP}$, and consists of expulsion of the 3D vortex shown in panel (c) from the bottom of the strip followed by entrance of a new vortex from the top of the strip and so on.

We notice that as seen from the top convex surface, the 3D vortex shown in Fig. 7(a) would be equivalent to a 2D antivortex -2D vortex pair, with flux entering at the left ($-\Phi_0$, 2D antivortex) and exiting at the right (Φ_0 , 2D vortex). The portion of the 3D vortex near the top curved surface is always perpendicular to the surface, though the field is applied parallel to the bottom surface. Differently from the bulk portion, these pieces of the total 3D vortex experience the component of magnetization $M_n \equiv B_n - H_n$ that is normal to the curved surface. This component is inhomogeneous, being both B_n and H_n inhomogeneous [see Fig. 6(d)], and, hence, generates a magnetic force F_M that rivals the current polarity dependent Lorentz force F_L . The component of magnetic force tangent to the top surface acting on the entering piece of the 3D vortex ($-\Phi_0$) on the left side can be approximately estimated as $F_M^{(Av)} \propto +\nabla_x M_n(x)$ and the one acting on the exiting piece (Φ_0) as $F_M^{(V)}(x) \propto -\nabla_x M_n(x)$. An example of spatial dependence of such a force as extracted from the calculated B_n and H_n of Fig. 6(d) is shown in Fig. 7(d) and also qualitatively sketched by arrows in panels (a) and (c). As it is seen, the magnetic force always opposes the displacement of the $-\Phi_0$ and $+\Phi_0$ pieces from their equilibrium position [as it is the one in panel (a)] but the force is weaker if a displacement toward the interior of the strip is involved. This explains the asymmetry of the critical currents in the mixed state. In fact, at negative critical current density $J = J_{CN}$ the F_L moves the $-\Phi_0$ and $+\Phi_0$ pieces toward the interior of the strip overcoming the weak F_M opposing the displacement, and eventually the whole 3D vortex exits from the top of the strip ($-\Phi_0$ and $+\Phi_0$ pieces annihilate) giving onset to dissipation. Conversely, at positive current density $J = |J_{CN}|$, the F_L moves the pieces toward the exterior but this time its strength is not enough to overcome the more strongly opposing F_M and the whole 3D vortex is only displaced, not ejected, as shown in panel (c). Hence, to eject the vortex and to establish dissipation a current density $J = J_{CP} > |J_{CN}|$ corresponding to a $F_L > F_M$ should be supplied.

In Fig. 8 we analyze the situation at a low magnetic field, $H = 0.07$, for which we are again in the Meissner state. In panel (a) is $J = 0$. In panel (b) we are at the negative criti-

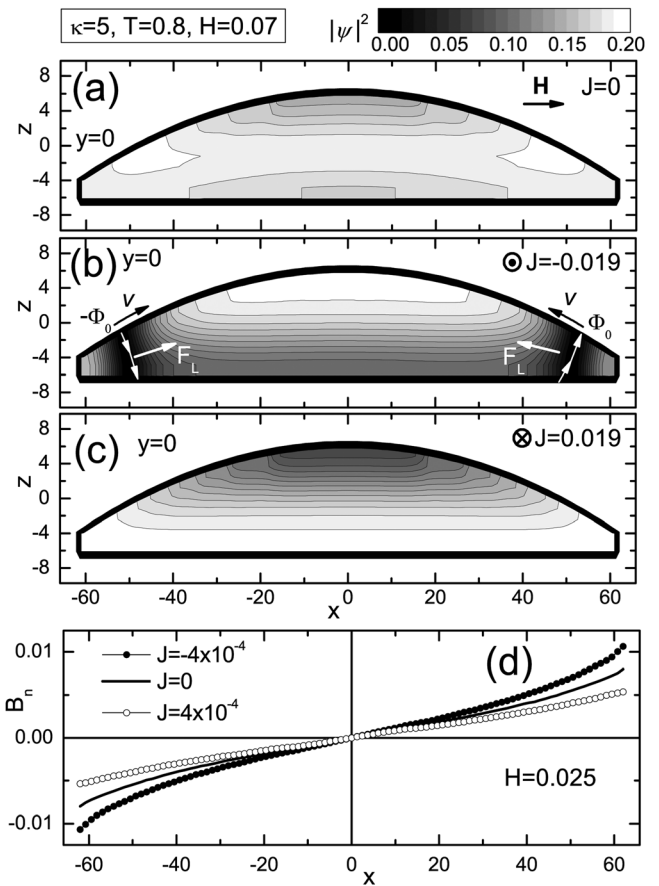


FIG. 8. Contour plots of the squared order parameter in the Meissner state. (a) $J = 0$. (b) Bias current corresponding to negative critical current, $J = J_{CN}$. (c) $J = |J_{CN}| < J_{CP}$. (d) Normal component of magnetic induction field B_n at positive, negative, and zero transport current density J . The external magnetic field is $H = 0.025$, falling in the Meissner regime.

cal current density, $J = J_{CN}$. The dynamical process accounting for dissipation is very similar to the one we discussed above, but for the initial stage. Here flux was not preexisting, and it enters the strip as a 3D antivortex at the left and a 3D vortex at the right. Under the action of F_L , the 3D V and 3D Av move inward until they join together to form again a vortex as the one in the Fig. 7(a). This vortex is expelled from the top surface, continuing the ever dynamic process. In Fig. 8(c) is $J = |J_{CN}|$. As it is seen, no flux is present and no dissipation is established. Hence, also starting with the strip in the Meissner state we again observe $J_{CP} > |J_{CN}|$, as in the experiment. At positive critical current, a 3D vortex enters from the top of the strip and the same dynamical process as the one we described above when the strip is in the mixed state and $J = J_{CP}$ is again established.

Inspection of panels (b) and (c) of Fig. 8 suggests that in the Meissner state the main mechanism of asymmetry involves the current polarity dependent self-field associated to the transport current density J . In panel (d) we show the normal component of the induction field, B_n , when the bias current density is negative, positive or zero. As it is seen, when $J < 0$ the self field cooperates with the applied field $H_n(x)$, so that the magnetic induction field $B_n(x)$ is larger than what the applied field $H_n(x)$ would generate by itself and at $J = J_{CN} < 0$ the $B_n(x)$ at the edges of the strip is large

enough to nucleate a 3D antivortex at left and a 3D vortex at right, as shown in panel (b), with onset of dissipation. Conversely, when the bias current density is positive, the self-field opposes to the external field $H_n(x)$, producing a $B_n(x)$ lower than what $H_n(x)$ would generate [see panel (d)]. This allows a positive bias current density $J_{CP} > |J_{CN}|$ to be fed into the strip before that, as discussed above, a 3D vortex enters from the top of the strip at the positive critical current density $J = J_{CP} > |J_{CN}|$, with associated onset of dissipation. From the above analysis we conclude that in the Meissner state the asymmetry is mainly due to the balance of polarity dependent self fields and the inhomogeneous normal component of external magnetic field.

IV. SUMMARY

Summarizing, we have reported the experimental and numerical investigation of magneto-transport properties of a Nb thin strip with plano-convex section. The strip exhibits a considerable asymmetry in the critical currents when the magnetic field is applied parallel to the substrate. An asymmetry ratio of critical currents as large as 300% has been observed at 4.2 K, that makes the single superconducting thin strip with tailored section possibly interesting for applications as a superconducting current rectifier at micron scale. The observed asymmetry has been ascribed to the inhomogeneous (antisymmetric) magnetic field component normal to the convex top surface of the strip. At low applied fields, the normal component can enhance or weaken the polarity dependent self-field of the bias current. At larger magnetic fields the asymmetry comes from the balance of the magnetic force due to the inhomogeneous normal component of

applied field and the polarity dependent Lorentz force associated to the transport current.

- ¹P. S. Swartz and H. R. Hart, *Phys. Rev.* **156**, 412 (1967).
- ²F. Raissi and J. E. Nordman, *Appl. Phys. Lett.* **65**, 1838 (1994).
- ³G. Carapella and G. Costabile, *Phys. Rev. Lett.* **87**, 077002 (2001).
- ⁴J. E. Villegas, S. Savelaev, F. Nori, E. M. Gonzalez, J. V. Anguita, R. Garcia, and J. L. Vicent, *Science* **302** 1188 (2003).
- ⁵K. Yu, T. W. Heitmann, C. Song, M. P. DeFeo, B. L. T. Plourde, M. B. S. Hesselberth, and P. H. Kes, *Phys. Rev. B* **76**, 220507(R) (2007).
- ⁶A. Yu. Aladyshkin, D. Yu. Vodolazov, J. Fritzsche, R. B. G. Kramer, and V. V. Moshchalkov, *Appl. Phys. Lett.* **97**, 052501 (2010).
- ⁷G. Carapella, P. Sabatino, and G. Costabile, *Phys. Rev. B* **81**, 054503 (2010).
- ⁸G. Carapella, V. Granata, F. Russo, and G. Costabile, *Appl. Phys. Lett.* **94**, 242504 (2009).
- ⁹D. Y. Vodolazov, B. A. Gribkov, A. Yu. Klimov, V. V. Rogov, and S. N. Vdovichev, *Appl. Phys. Lett.* **94**, 012508 (2009).
- ¹⁰D. Y. Vodolazov, B. A. Gribkov, S. A. Gusev, A. Yu. Klimov, Yu. N. Nozdrin, V. V. Rogov, and S. N. Vdovichev, *Phys. Rev. B* **72**, 064509 (2005).
- ¹¹A. Papon, K. Senapati, and Z. H. Barber, *Appl. Phys. Lett.* **93**, 172507 (2008).
- ¹²M. Morelle and V. V. Moshchalkov, *Appl. Phys. Lett.* **88**, 172507 (2006).
- ¹³M. Tinkham, *Introduction to Superconductivity* (McGraw-Hill, Singapore, 1996).
- ¹⁴M. Machida and H. Kaburaki, *Phys. Rev. Lett.* **71**, 3206 (1993).
- ¹⁵T. Winiecki and C. S. Adams, *Phys. Rev. B* **65**, 104517 (2002).
- ¹⁶T. Winiecki and C. S. Adams, *J. Comput. Phys.* **179**, 127 (2002).
- ¹⁷D. Y. Vodolazov and F. M. Peeters, *Phys. Rev. B* **76**, 014521 (2007).
- ¹⁸D. Y. Vodolazov, F. M. Peeters, M. Morelle and V. V. Moshchalkov, *Phys. Rev. B* **71**, 184502 (2005).
- ¹⁹L. P. Gorkov, *Sov. Phys. JETP* **36**, 1364 (1959).
- ²⁰K. Ohnishi, T. Kimura, and Y. Otani, *Appl. Phys. Exp.* **1**, 021701 (2008).
- ²¹P. Sabatino, C. Cirillo, G. Carapella, M. Trezza, and C. Attanasio, *J. Appl. Phys.* **108**, 053906 (2010).
- ²²D. Y. Vodolazov and I. L. Maksimov, *Physica C* **349**, 125 (2001).
- ²³W. H. Press, S. A. Teukolsky, W. T. Vetterling, and B. P. Flannery, *Numerical Recipes: The Art of Scientific Computing* (Cambridge University Press, 2007), 3rd ed.
- ²⁴E. H. Brandt, *Phys. Rev. B* **48**, 6699 (1993).